MULTI-BAND PERFECT ABSORPTION INDUCED BY BREAKING THE SYMMETRY OF METAMATERIAL STRUCTURE

Dinh Hong Tiep[1, 2], Bui Son Tung[2], Bui Xuan Khuyen[2], Vu Dinh Lam[1, *]

[1]*Graduate University of Science and Technology, Vietnam Academy of Science and Technology, 18 Hoang Quoc Viet str., Cau Giay, Ha Noi*

[2]*Institute of Materials Science, Vietnam Academy of Science and Technology, 18 Hoang Quoc Viet str., Cau Giay, Ha Noi*

[*]Email: *lamvd@gust-edu.vast.vn*

Abstract. In this work, a multi-band metamaterial perfect absorber is demonstrated numerically and experimentally in the microwave region based on the breaking symmetry of geometrical structure. Initially, when the structure, which is designed in the X shape, is in the symmetric geometry, only one absorption peak is observed. By breaking the symmetry of structure, new absorption peaks emerge, leading to the multi-band perfect absorption. In addition, the separations of absorption peaks are proportional to the degree of geometrical asymmetry. Our work presents a simple and efficient approach to create multi-band metamaterial perfect absorbers.

Keywords: metamaterial perfect absorber, multi-band, breaking symmetry.

Classification numbers: 2.1.2, 2.2.2, 2.8.2.

1. INTRODUCTION

More than ten years ago, the first metamaterial perfect absorber (MPA) was demonstrated in 2008 by Landy *et al.* [1]. By adjusting the geometrical parameters of artificial unit-cell, the electric and magnetic responses of the MPA are controlled to achieve the perfect absorption at microwave frequency. At the interested frequency, the impedance of the MPA, which is defined by $Z = \sqrt{\mu/\varepsilon}$, is matched well to that of the surrounding environment, leading to the elimination of reflection of incoming electromagnetic wave. In addition, the strong resonance behavior at absorption frequency confines the energy inside the MPA structure, leading to the minimum of transmission. Consequently, all energy of incoming wave is absorbed perfectly by the MPA. Afterward, researchers demonstrated many MPAs operating at various frequency ranges such as MHz [2, 3], GHz [4-8], THz [9, 10], infrared [11-13], and optical [14, 15] regions. So far, there are two main research trends related to the MPA. The first one focuses on how to control the absorption behavior actively by using the external thermal [16], electrical [17], magnetic [18] or optical [19] impacts. The second one is the study for the multi-band [20] and broadband MPAs

[21]. Because the nature of MPAs is based on resonance phenomenon, the perfect absorption of MPA is basically limited to a narrow frequency region. Therefore, the extension of absorption bandwidth is a necessary study and should be conducted.

In this work, we propose a simple and efficient way to create the multi-band absorption by breaking the symmetry of metamaterial structure. Owing to the asymmetry of MPA, the new absorption peaks arise in addition to the initial absorption peak of symmetric structure. The result might contribute another method to create the multi-band MPAs.
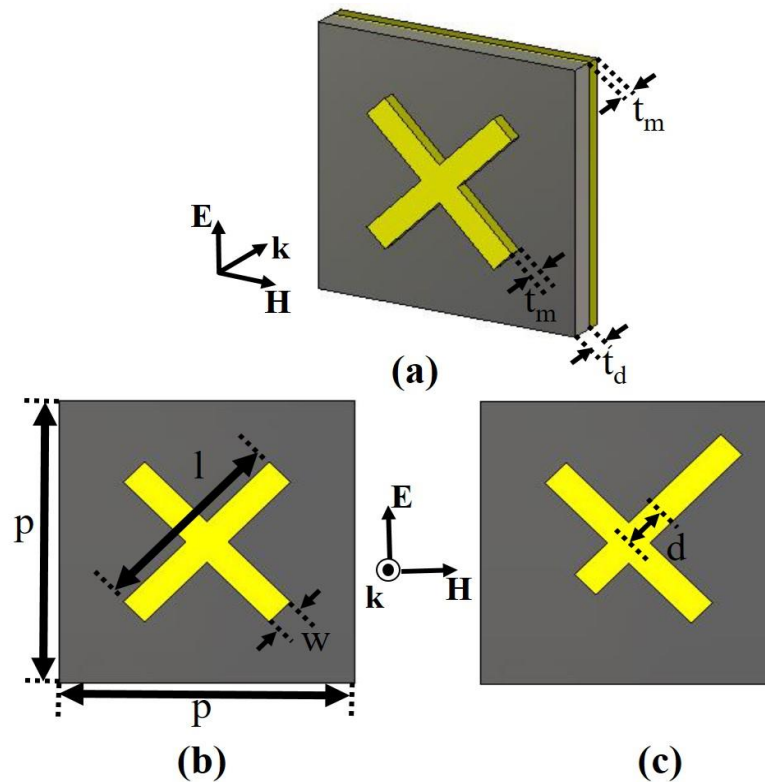
2. DESIGN AND SIMULATION

Figure 1. Illustration of unit cell of MPA: (a) perspective view, (b) front view for the symmetric structure and (c) front view for the asymmetric structure with the displacement d.

Figure 1 shows designed unit-cell of proposed MPA with X-shape patterned structure. The proposed MPA consists of three layers: the front metallic patterned layer, the middle dielectric layer and the back continuous metallic layer. The thicknesses of the metallic and the dielectric layers are t_d = 1.2 mm and t_m = 0.035 mm, respectively. The other geometrical parameters of MPA structure are l = 7 mm, w = 0.3 mm, and p = 10 mm. In simulation, the metallic layers are made of copper with the electrical conductivity of 5.6×10^7 S/m. The dielectric space is chosen as FR-4 with the dielectric constant of 4.3 and the loss tangent of 0.025.

The commercial software CST Microwave Studio [22], which is based on the finite integration technique (FIT), is exploited to simulate the electromagnetic behavior of the MPA. The unit-cell boundary is applied to present the periodicity of the unit-cell. The electric and magnetic fields are polarized along the side lengths of unit-cell, respectively. The wave vector is

normal to the plane of MPA structure with the propagation direction from the front patterned layer to the back continuous layer. The absorption of MPA is expressed as:

$$A(\omega) = 1 - |S_{11}(\omega)|^2 - |S_{21}(\omega)|^2, \tag{1}$$

where $S_{11}(\omega)$ and $S_{21}(\omega)$ are the reflection and the transmission parameters, respectively. Because the back layer of MPA is copper, which is perfect conductor in the microwave region, the transmission is forbidden. Consequently, the absorption of MPA is simplified to be:

$$A(\omega) = 1 - |S_{11}(\omega)|^2. \tag{2}$$

The conventional printed-circuit-board method was used to fabricate the MPA samples. A multi-layer film, which is composed of a 1.2-mm-thick FR-4 layer between two 0.035-mm-thick copper layers, is coated by photoresist on one side. After putting a mask of designed structure on the coated side of film, the photolithography process was carried out. Finally, the exposed part of copper layer was removed by the wet-etching technique, revealing the structural pattern. The absorption spectrum was measured by a vector network analyzer connected to linearly-polarized microwave standard-gain horn antennas. The experiment process was performed in a microwave anechoic chamber. To satisfy the far-field condition, antennas and sample were separated by 2.0 m from each other (the separated distance is around 60 times larger than the absorption wavelength).
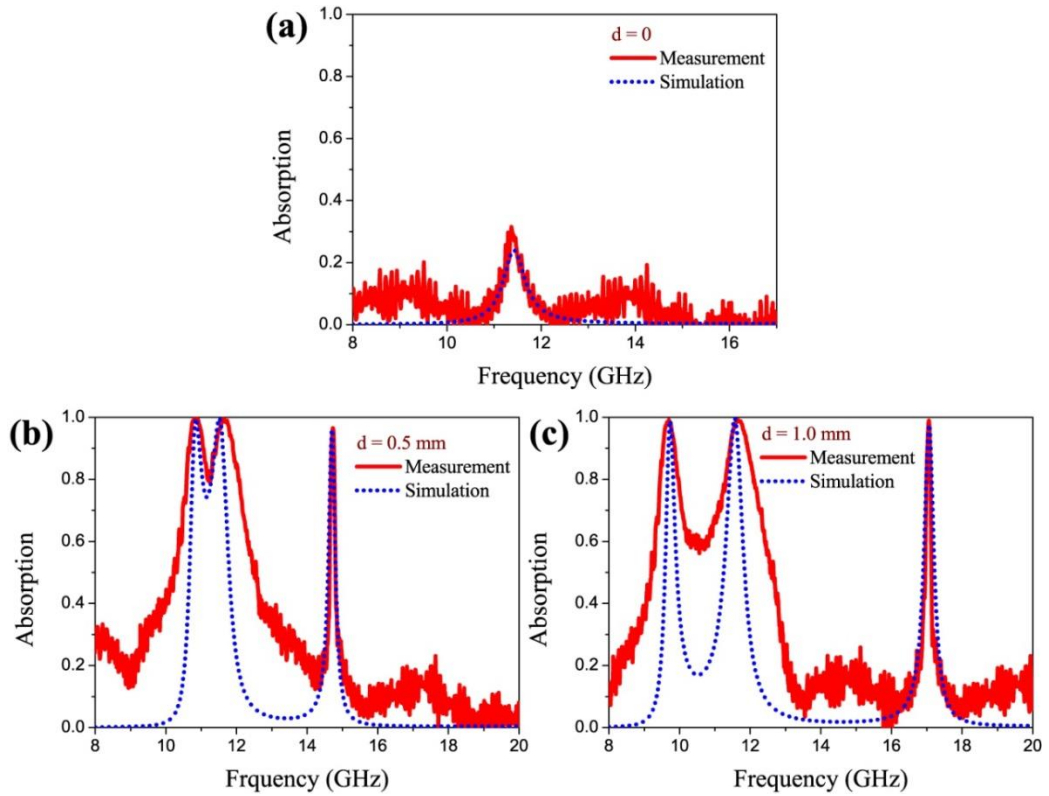
3. RESULTS AND DISCUSSION

Figure 2. Simulated and measured absorption spectra of MPA for (a) d = 0, (b) d = 0.5 and (c) d = 1.0 mm.

Figure 2 shows the absorption spectra for different displacements of the cut-wire (CW) in X-shape structure. Here, one CW is displaced along the diagonal direction while the other CW is fixed. For the simulation, it is shown that for the initial symmetric MPA (d = 0), there is only one absorption peak of 24 % at 11.4 GHz. By adjusting the position of CW to d = 0.5 mm, two new absorption peaks arise, creating a triple-band absorption with the absorption frequencies of 10.8, 11.5 and 14.7 GHz. The absorption magnitudes of the first, the second and the third peaks are 99 %, 99 % and 95 %, respectively. The absorption peaks are separated further when the displacement d is increased. At d = 1.0 mm, the absorption frequencies are 9.7, 11.6 and 17.1 GHz while the absorption magnitudes are kept to be 99 %, 100 % and 97 %, respectively. The simulation and the experiment are in good agreement, especially at the absorption resonance frequency. Outside the resonance regions, there are slight mismatches between the simulated and the measured spectra, which can be explained due to the imperfection of measurement condition.

To understand the absorption mechanism of the triple-band MPA, the surface currents on metallic layers at absorption frequencies are simulated for d = 0 and d = 1 mm, as shown in Fig. 3. For the symmetric structure d = 0, the surface currents on the front and the back copper layers are antiparallel, which indicates the existence of a magnetic resonance at absorption frequency.
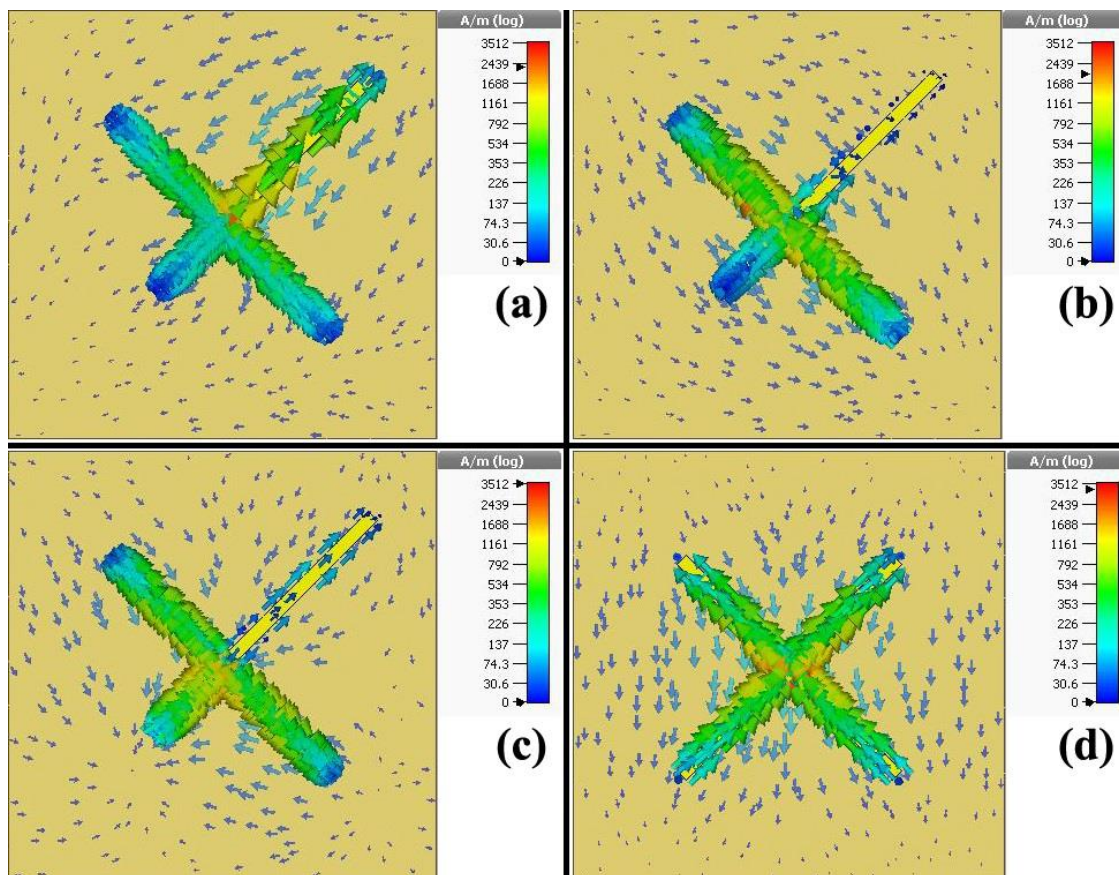

Figure 3. Surface currents on the front and the back metallic layers of asymmetric MPA (d = 1.0 mm) at absorption frequencies (a) 9.7, (b) 11.6 and (c) 17.1 GHz. (d) Surface currents on the front and the back metallic layers of symmetric MPA (d = 0) at absorption frequency of 11.4 GHz.

Therefore, the magnetic resonance is the mechanism of the nearly perfect absorption at 11.4 GHz. For the asymmetric structure d = 1 mm, the surface currents on copper layers are also antiparallel. It suggests that the mechanism of absorption is still magnetic resonance. However, the distributions of surface currents are changed at different absorption frequencies and they are also different to the distribution of surface currents in the symmetric state. The differences on the absorption modes can be understood further by considering the surface current on the front X shape layer. At the first absorption frequency of asymmetric MPA, the surface current is strongly induced on longer half of the displaced CW and on center part of the fixed CW. On the other hand, the current is mostly excited on shorter half of the displaced CW and on center part of the fixed CW at the third absorption frequency. For the second absorption frequency, the surface current is induced mainly on the fixed CW. This is the reason why the second absorption frequency of asymmetric MPA is nearly same as the absorption frequency of the symmetric MPA. In addition, by considering the flowing length of strong current, it can be seen that the flowing length of surface current at the first absorption mode is longer than that of the second absorption mode, while the flowing length of surface current at the third absorption mode is shorter than that of the second absorption mode. Because the flowing length of surface current defines the inductance of the structure, which is inversely proportional to the magnetic resonance frequency, the first absorption mode happens at lowest frequency and the third absorption mode occurs at highest frequency on the triple-band absorption. To observe clearly the contribution of magnetic resonance to the multi-band absorption, the magnetic field distribution is simulated at absorption frequencies, as shown in Fig. 4.
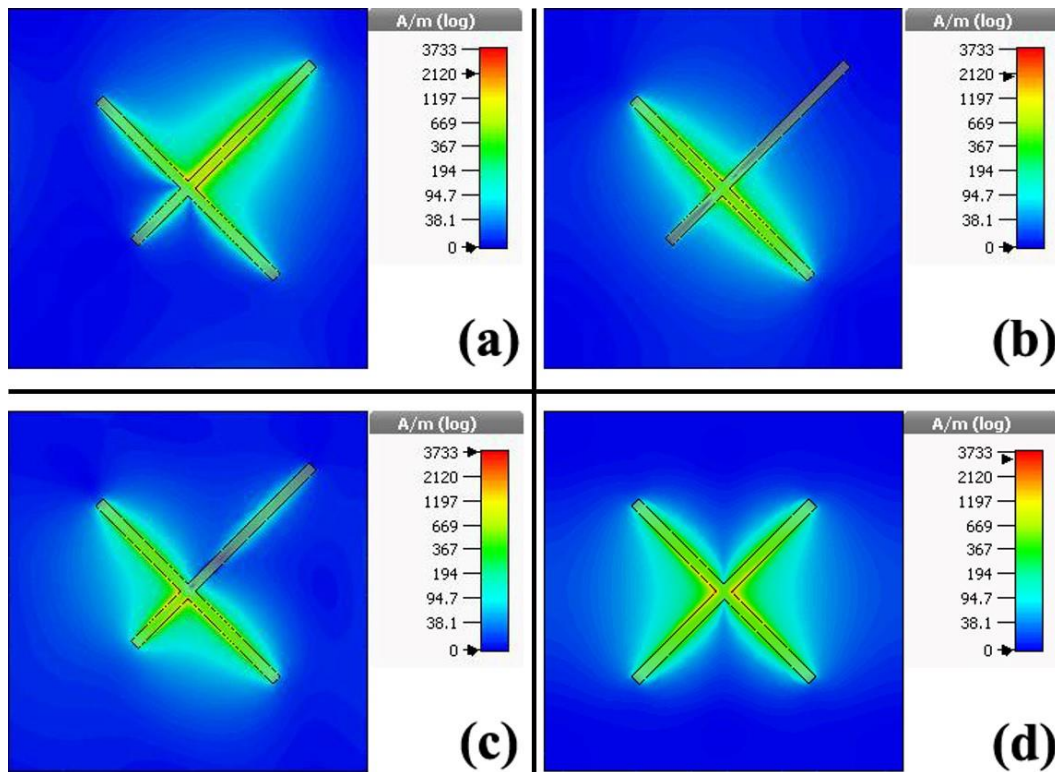
Figure 4. Magnetic field distribution on asymmetric MPA (d = 1.0 mm) at absorption frequencies (a) 9.7, (b) 11.6 and (c) 17.1 GHz. (d) Magnetic field distribution on symmetric MPA (d = 0) at absorption frequency of 11.4 GHz.

The simulation shows that magnetic fields are strongly excited in the MPA at the absorption frequencies, which confirmed directly the magnetically resonant nature of absorption. Because the magnetic field is related to the induced current, the distribution of magnetic field can represent the effective region of equivalent inductance in magnetic resonance. The magnetic fields are located strongly at the position corresponding to the longer half of the displaced CW, the fixed CW and the shorter half of the displaced CW at 9.7, 11.6 and 17.1 GHz, respectively. The observed results are in agreement with the simulated surface currents in Fig. 3. It is noteworthy that although the region of magnetic field in the symmetric MPA is large, the contribution of effective impedance is different to asymmetric MPA. Therefore, the magnetic resonance frequency is excited at 11.4 GHz.

4. CONCLUSIONS

In summary, we proposed a method to create the multi-band MPA by breaking the symmetry of structure. Due to the asymmetry of geometrical structure, the initial single-band absorption of symmetric MPA is transformed to the triple-band absorption of asymmetric MPA. It is also clarified that the asymmetric structure induces different current distributions at different absorption frequencies, which decide the frequencies of absorption modes. Our work might contribute a simple approach to create multi-band MPAs which are suitable to applications in multi-channel sensors, filters and multiplexers.

REFERENCES

1. Landy N. I., Sajuyigbe S., Mock J. J., Smith D. R., and Padilla W. J. - Perfect metamaterial absorber, Phys. Rev. Lett. **100** (2008) 207402.

2. Khuyen B. X., Tung B. S., Yoo Y. J., Kim Y. J., Kim K. W., Chen L.-Y., Lam V. D., and Lee Y. P. - Miniaturization for ultrathin metamaterial perfect absorber in the VHF band, Sci. Rep. **7** (2017) 45151.

3. Khuyen B. X., Tung B. S., Kim Y. J., Hwang J. S., Kim K. W., Rhee J. Y., Lam V. D., Kim Y. H., and Lee Y. P. - Ultra-subwavelength thickness for dual/triple-band metamaterial absorber at very low frequency, Sci. Rep. **8** (2018) 11632.

4. Tung B. S., Khuyen B. X., Kim Y. J., Lam V. D., Kim K. W., and Lee Y. P. - Polarization-independent, wide-incident-angle and dual-band perfect absorption, based on near-field coupling in a symmetric metamaterial, Sci. Rep. **7** (2017) 11507.

5. Kim Y. J., Hwang J. S., Khuyen B. X., Tung B. S., Kim K. W., Rhee J. Y., Chen L.-Y., and Lee Y. P. - Flexible ultrathin metamaterial absorber for wide frequency band, based on conductive fibers, Sci. Technol. Adv. Mater. **19** (1) (2018) 711-717.

6. Hoa N. T. Q., Tuan T. S., Hieu L. T., and Giang B. L. - Facile design of an ultra-thin broadband metamaterial absorber for C-band applications, Sci. Rep. **9** (2019) 468.

7. Kalraiya S., Chaudhary R. K., and Abdalla M. A. - Design and analysis of polarization independent conformal wideband metamaterial absorber using resistor loaded sector shaped resonators, J. Appl. Phys. **125** (2019) 134904.

8. Zhou Q., Yin X., Ye F., Mo R., Tang Z., Fan X., Cheng L., and Zhang L. - Optically transparent and flexible broadband microwave metamaterial absorber with sandwich structure, Appl. Phys. A **125** (2019) 131.

9. Xu W., Xie L., Zhu J., Tang L., Singh R., Wang C., Ma Y., Chen H.-T., and Ying Y. - Terahertz biosensing with a graphene-metamaterial heterostructure platform, Carbon **141** (2019) 247-252.

10. Huang L., Chowdhury D. R., Ramani S., Reiten M. T., Luo S.-N., Taylor A. J., and H. T. Chen - Experimental demonstration of terahertz metamaterial absorbers with a broad and flat high absorption band, Opt. Lett. **37** (2) (2012) 154-156.

11. Ghaderi M., Shahmarvandi E. K., and Wolffenbuttel R. F. - CMOS-compatible mid-IR metamaterial absorbers for out-of-band suppression in optical MEMS, Opt. Mater. Express **8** (7) (2018) 1696-1707.

12. Ding F., Dai J., Chen Y., Zhu J., Jin Y., and Bozhevolnyi S. I. - Broadband near-infrared metamaterial absorbers utilizing highly lossy metals, Sci. Rep. **6** (2016) 39445.

13. Yi Z., Lin H., Niu G., Chen X., Zhou Z., Ye X., Duan T., Yi Y., Tang Y., and Yi Y. - Graphene-based tunable triple-band plasmonic perfect metamaterial absorber with good angle-polarization-tolerance, Results Phys. **13** (2019) 102149.

14. Hao J., Wang J., Liu X., Padilla W. J., Zhou L., and Qiu M. - High performance optical absorber based on a plasmonic metamaterial, Appl. Phys. Lett. **96** (2010) 251104.

15. Wang W., Qu Y., Du K., Bai S., Tian J., Pan M., Ye H., Qiu M., and Li Q. - Broadband optical absorption based on single-sized metal-dielectric-metal plasmonic nanostructures with high-ε'' metals, Appl. Phys. Lett. **110** (2017) 101101.

16. Yang L., Zhou P., Huang T., Zhen G., Zhang L., Bi L., Weng X., Xie J., and Deng L. - Broadband thermal tunable infrared absorber based on the coupling between standing wave and magnetic resonance, Opt. Mater. Express **7** (8) (2017) 2767-2776.

17. Savo S., Shrekenhamer D., and Padilla W. J. - Liquid Crystal Metamaterial Absorber Spatial Light Modulator for THz Applications, Adv. Optical Mater. **2** (2014) 275–279.

18. Wang W., Wang J., Yan M., Wang J., Ma H., Feng M., Qu S. - Dual band tunable metamaterial absorber based on cuboid ferrite particles, J. Phys. D: Appl. Phys. **51** (2018) 315001.

19. Zhao X., Wang Y., Schalch J., Duan G., Cremin K., Zhang J., Chen C., Averitt R. D., and Zhang X. - Optically modulated ultra-broadband all-silicon metamaterial terahertz absorbers, ACS Photonics (2019) DOI: 10.1021/acsphotonics.8b01644.

20. Dung N. V., Tung B. S., Khuyen B. X., Yoo Y. J., Kim Y. J., Rhee J. Y., Lam V. D., and Lee Y. P. - Simple metamaterial structure enabling triple-band perfect absorber, J. Phys. D: Appl. Phys. **48** (2015) 375103.

21. Tiep D. H., Khuyen B. X., Tung B. S., Kim Y. J., Hwang J. S., Lam V. D., and Lee Y. P. - Enhanced-bandwidth perfect absorption based on a hybrid metamaterial, Opt. Mater. Express **8** (9) (2018) 2751-2759.

22. http://www.cst.com. CST of America, Inc., 492 Old Connecticut Path, Suite 505 Framingham, MA 01701, USA.